Inorg. Chem. **2009**, *48*, 557−564

Luminescent and Structural Properties of $(Sr_{1-x},Ba_x)_3MgSi_2O_8:Eu^{2+}$: Effects of Ba Content on the Eu^{2+} Site Preference for Thermal Stability

Won Bin Im,[†,‡] Yong-Il Kim,[§] Hyoung Sun Yoo,[‡] and Duk Young Jeon*[,‡]

Department of Materials Science and Engineering, Korea Advanced Institute of Science and Technology, Daejeon, 305-701, Republic of Korea, and Korea Research Institute of Standards and Science, P.O. Box 102, Yuseong, Daejeon, 305-600, Republic of Korea

Received July 8, 2008

A blue-color-emitting phosphor, $(Sr_{1-x},Ba_x)_3MgSi_2O_8:Eu^{2+}$ ($SB_xMS:Eu^{2+}$), with various Ba contents, was synthesized, and its thermal stability was evaluated. Depending upon the Ba content, the dominant emission wavelength of the $SB_xMS:Eu^{2+}$ phosphor could be tuned, and good photoluminescence (PL) properties were obtained under an excitation by a 147 nm source. The PL behavior showed that the thermal stability of $SB_xMS:Eu^{2+}$ baked at 500 °C was dependent upon the Ba content. On the basis of the results of electron spin resonance on Eu^{2+} and Rietveld refinement against neutron powder diffraction data of the phosphor, it was found that the improved thermal stability of $SB_xMS:Eu^{2+}$ could be ascribed to Eu^{2+} occupying preferred Sr sites among three possible locations depending upon the amount of Ba substitution. It is also inferred from this observation that the average interatomic distances between Eu^{2+} and O (d_{Eu-O}) of the different Sr sites may play an important role in the thermal stability of the phosphor.

1. Introduction

At present, plasma display panels (PDPs) are the most popular devices among large-area flat panel display devices. However, the performance of PDPs still requires improvement with respect to efficiency and lifetime. In particular, these properties are closely related to phosphors excited by vacuum ultraviolet (VUV) energy, which is generated by Xe plasma discharge, as the excitation source of phosphors. Because phosphors convert VUV photons to visible light, enhancement of the luminous efficiency is a key issue for PDP phosphors.[1−6]

Therefore, much attention has been paid to finding new or advanced color-emitting phosphors so as to improve the performance of PDPs. As far as the development of phosphors is concerned, Eu^{2+} ions were used frequently as an activator ion for various host lattices. This occurs because the $4f^7$ electron configuration of the Eu^{2+} ion shows efficient luminescence owing to the 4f → 5d transition, and the luminescence colors or wavelengths change widely from near-ultraviolet to red regions depending upon the nature of a host lattice. In particular, Eu ions usually exist in a trivalent oxidation state in various compounds. Under reducing conditions, Eu^{2+} ions can be stable on alkaline earth sites. However, when Eu^{2+} ions are heated within a certain temperature range in the air, they may be oxidized as follows:

$$Eu^{2+} \rightarrow Eu^{3+} + e^-$$

Therefore, there is a luminescence decrease of the Eu^{2+}-activated phosphor during the PDP manufacturing process, in which the phosphor layer formed by screen printing goes through several heat treatments up to 500 °C in the air. That is, such a thermal history has a large impact on the thermal

* To whom correspondence should be addressed. Tel.: +82-42-869-3337. Fax: +82-42-869-3310. E-mail: dyj@kaist.ac.kr.
† Current address: Solid State Lighting and Energy Center, Materials Department, and Materials Research Laboratory, University of California, Santa Barbara, CA 93106, E-mail: imwonbin@mrl.ucsb.edu.
‡ Korea Advanced Institute of Science and Technology.
§ Korea Research Institute of Standards and Science.

(1) Do, Y. R.; Park, D. H.; Kim, Y. S. *J. Electrochem. Soc.* **2004**, *151* (10), H210.
(2) Chen, K.-F.; Ostrom, N. P.; Park, S.-J.; Eden, J. G. *Appl. Phys. Lett.* **2006**, *88*, 061121.
(3) Kim, J. S.; Yang, J. H.; Kim, T. J.; Whang, K. W. *IEEE Trans. Plasma Sci.* **2003**, *31*, 1083.
(4) Kunimoto, T. Yoshimatsu, R.; Hhmi, K.; Tanaka, S.; Kobayashi, H. K. *IEICE Trans. Electron.* **2002**, *E85-C*, 11.
(5) Jung, K. Y.; Lee, H. Y.; Kang, Y. C.; Park, S. B.; Yang, Y. S. *Chem. Mater.* **2005**, *17*, 2729.
(6) Im, W. B.; Kim, Y.-I.; Kang, J. H.; Jeon, D. Y. *Solid State Commun.* **2005**, *134*, 177.

10.1021/ic8012798 CCC: $40.75
Published on Web 12/18/2008

Table 1. PL Behaviors of Various Phosphors after Baking Process at 500 °C

phosphor	crystal structure	ΔI (=[(I_{fresh} − I_{baked})/I_{fresh}] × 100)	Interatomic distance (Å):d_{Eu-O}
BAM:Eu^{2+}	hexagonal	25%	2.942
H-BAS:Eu^{2+}[13]	hexagonal	34%	3.114
M-BAS:Eu^{2+}[13]	monoclinic	0%	2.934
KBP:Eu^{2+}	orthorhombic	7%	2.822
LAM:Eu^{2+}	hexagonal	2%	2.734
CMS:Eu^{2+}[14,15]	monoclinic	0%	2.497
CAS:Eu^{2+}[16]	triclinic	8%	≈2.8

stability of a color-emitting phosphor.[4,6,7] Therefore, Eu^{2+}-activated phosphors are desired to have a high thermal stability for PDP application during the baking process.

For example, the thermal stability of blue-emitting $BaMgAl_{10}O_{17}:Eu^{2+}$ (BAM:Eu^{2+}), less stable than red-emitting or green-emitting counterparts, has been studied intensively, particularly after the baking process at 500 °C in the air for 30 min. There have been many attempts to understand the origin of the observed thermal stability of BAM:Eu^{2+}.[7−12] Many aspects have been discovered; however, we are still far from a complete understanding. In addition, there are almost no in-depth studies related to the thermal stability of phosphors except BAM:Eu^{2+}. Furthermore, to develop a new color-emitting phosphor for PDP application, certain criteria are needed to select a host lattice having a strong thermal stability for Eu^{2+} ions.

On the basis of this motivation, we have studied the thermal stability of several blue-emitting PDP phosphors and obtained experimental results indicating that the crystal structure of a host lattice might have large influence on its thermal stability during the baking process. Through the study utilizing a polymorph of $BaAl_2Si_2O_8:Eu^{2+}$, it was suggested that the average interatomic distances (d_{Eu-O}) between Eu^{2+} and the neighboring oxygen being short could be considered as an important factor in a host lattice showing thermal stability during the baking process.[13]

In order to check the validity of this hypothesis, we have further evaluated various phosphor systems such a $LaMgAl_{11}O_{19}:Eu^{2+}$ (LAM:Eu^{2+}), $CaMgSi_2O_6:Eu^{2+}$ (CMS:Eu^{2+}), and $CaAl_2Si_2O_8:Eu^{2+}$ (CAS:Eu^{2+}) and compared the phosphors with a commercial BAM:Eu^{2+} phosphor.[14−16] Table 1 shows the result of a thermal stability test on various phosphor systems. As shown in Table 1, it seemed that phosphors having the shorter d_{Eu-O} showed stronger thermal stability in comparison with the BAM:Eu^{2+} phosphor due to the Eu^{2+} ion, which may be protected from an outer oxidation atmosphere successfully. In addition, from checking the various phosphor systems in terms of the thermal stability, our proposed mechanism seems to work well.

On the basis of this information, the $(Sr_{1-x},Ba_x)_3MgSi_2O_8$ (SB_xMS) phosphor was selected as a host lattice for the Eu^{2+} activator. Because SB_xMS does not have an open layer in the host lattice and its structure has three different sites for Eu^{2+} ions, it is suitable in terms of our previous findings about the interatomic distance between the Eu^{2+} ion and its neighboring oxygen ions. With consideration of structural information, we have studied the present $(Sr_{1-x},Ba_x)_3MgSi_2O_8:Eu^{2+}$ ($SB_xMS:Eu^{2+}$) phosphor with various Ba contents and evaluated its thermal stability. Furthermore, the cause of the thermal degradation of $SB_xMS:Eu^{2+}$ was investigated using electron spin resonance (ESR) and Rietveld refinement against its neutron powder diffraction data. To investigate Ba substitution sites in the host lattice, geometry optimization calculations for each given Eu site were performed with the Cambridge Serial Total Energy Package (CASTEP) code, which employs density functional theory, pseudopotential, and a plane-wave basis set to provide a good atomic-level description of all manners of materials and molecules. Consequently, this study investigates the variation in thermal stability of $SB_xMS:Eu^{2+}$ added with Ba after the baking process and introduces a new blue-emitting phosphor for PDP application.

2. Experimental Section

2.1. Sample Preparation. Powder samples of $SB_xMS:Eu^{2+}$ were prepared by a solid-state reaction method. To synthesize the phosphor samples, $SrCO_3$ (Aldrich, 99.99%), $BaCO_3$ (Aldrich, 99.99%), MgO (Aldrich, 99.99%), SiO_2 (Kojundo, 99.99%), and Eu_2O_3 (Aldrich, 99.99%) were used as raw materials. In this study, through the optimization process of an activator ion, the concentration of Eu^{2+} was fixed to 0.02 mol for Sr elements. The raw materials were mixed using an agate mortar for 1 h and subsequently heated in a temperature range of 1300−1400 °C in a reducing atmosphere of H_2 (5%) and N_2 (95%) for 3 h.

2.2. Photoluminescence (PL) Measurement. The emission spectra of $SB_xMS:Eu^{2+}$ were obtained using a standard DARSA PRO PL System (Professional Scientific Instrument Co, Korea) spectrometer, which utilizes a deuterium lamp as an excitation source. The sample chamber was maintained at about 5×10^{-5} torr using a turbo pump. PL spectra were obtained in a wavelength region scanned from 360 to 600 nm under excitation of 147 nm radiation from the deuterium lamp at room temperature. The excitation spectrum in the VUV region was corrected by sodium salicylate. In order to investigate the effect of the baking process on the luminescent property of $SB_xMS:Eu^{2+}$, the phosphor samples were baked at 500 °C in the air for 30 min and compared with one another.

2.3. Structural Analysis of $SB_xMS:Eu^{2+}$ Phosphor. Neutron powder diffraction data of the $SB_xMS:Eu^{2+}$ phosphor were collected over scattering angles ranging from 0° to 140° using 1.8348 Å neutrons on a high-resolution powder diffractometer at the Hanaro Center of the Korea Atomic Energy Research Institute. The General Structure Analysis System (GSAS) program was used to perform

(7) Oshio, S.; Matsuoka, T.; Tanaka, S.; Kobayashi, H. *J. Electrochem. Soc.* **1998**, *145*, 3903.
(8) Sohn, K. S.; Kim, S. S.; Park, H. D. *Appl. Phys. Lett.* **2002**, *81* (10), 1759.
(9) Kim, K.-B.; Kim, Y.-I.; Chun, H.-G.; Cho, T.-Y.; Jung, J.-S.; Kang, J.-G. *Chem. Mater.* **2002**, *14*, 5045.
(10) Kim, Y. -I.; Kim, K.-B.; Jung, M.-J.; Hong, J.-S. *J. Lumin.* **2002**, *99*, 91.
(11) Zhang, S.; Kono, T.; Ito, A.; Yasaka, T.; Uchiike, H. *J. Lumin.* **2004**, *106*, 39.
(12) Dawson, B.; Ferguson, M.; Marking, G.; Diaz, A. L. *Chem. Mater.* **2004**, *16*, 5311.
(13) Im, W. B.; Kim, Y.-I.; Jeon, D. Y. *Chem. Mater.* **2006**, *18*, 1190.
(14) Im, W. B.; Kang, J. H.; Lee, D. C.; Lee, S.; Jeon, D. Y.; Kang, Y. C.; Jung, K. Y. *Solid State Commun.* **2005**, *133*, 197.
(15) Im, W. B.; Kim, Y.-I.; Jeon, D. Y. *J. Mater. Res.* **2005**, *20*, 2061.
(16) Im, W. B.; Kim, Y.-I.; Jeon, D. Y. *Solid State Commun.* **2005**, *134*, 717.

the Rietveld refinement on the diffraction data.[17] A pseudo-Voigt function was chosen as a profile function among the profile functions available in GSAS.

2.4. Electron Spin Resonance Analysis. To analyze the change in Eu^{2+} ion sites, ESR (JES-FA200) measurements were carried out at the X-band frequency at room temperature. These measurements were expected to help to provide insight into the behavior of Eu^{2+} ions at room temperature.

2.5. Geometry Optimization Calculation with CASTEP. The geometric optimization calculation was done using CASTEP, developed by Payne et al.[18] The CASTEP code employs the plane-wave basis set to treat valence electrons and pseudopotentials to approximate the potential field of ion cores. Both the plane-wave basis set and the pseudopotentials are efficient tools used in density functional theory (DFT) and are especially suitable for calculations involving geometric optimization for various structures. The ultrasoft pseudopotentials and Perdew−Burke−Ernzerhof generalized gradient approximation functions were used for all calculations.[19] The energy cutoff was set to be above 310 eV for every element of SB_xMS phosphor. Parameters for convergence control of the geometry optimization were 0.2×10^{-5} eV/atom for total energy, 0.05 eV/Å for maximum force, 0.1 GPa for stress, and 0.002 Å for displacement. The Momkhuorst−Pack scheme was used to produce a uniform grid of k points along the three axes in reciprocal space.[20]

3. Results and Discussion

3.1. Luminescent Properties of $SB_xMS:Eu^{2+}$ Phosphor. The excitation and emission spectra of $SB_0MS:Eu^{2+}$ are shown in Figure 1a. In the PL spectra, the emission peak of $SB_0MS:Eu^{2+}$ was centered at about 460 nm. Its emission band corresponds to the transition from the $4f^65d$ excited state to the $4f^7$ ground state of a Eu^{2+} ion. Because of the strong crystal field around Eu^{2+} ions, the lowest 5d level would become lower than the $^6P_{7/2}$ level.[21] Although the optimization procedures were not performed perfectly, the initial PL intensity of $SB_0MS:Eu^{2+}$ was about 75% of that of a commercial $BAM:Eu^{2+}$ under VUV excitation. The obtained CIE color coordinates of the synthesized $SB_0MS:Eu^{2+}$ were $x = 0.157$ and $y = 0.083$. Figure 1b shows the dominant wavelength of $SB_xMS:Eu^{2+}$ depending upon Ba content. With an increase in Ba content, a change of the emission band to shorter wavelengths was observed. This may be attributed to changes in the crystal field around Eu^{2+} with the addition of Ba. Although the 4f electrons of Eu^{2+} are not sensitive to their surroundings due to shielding by the electrons present in the outer shell, the 5d electrons are split by the crystal field, which may lead to a shift in the emission peak of $SB_xMS:Eu^{2+}$.[22] In a $SB_xMS:Eu^{2+}$ phosphor system, the dominant emission wavelength could be easily

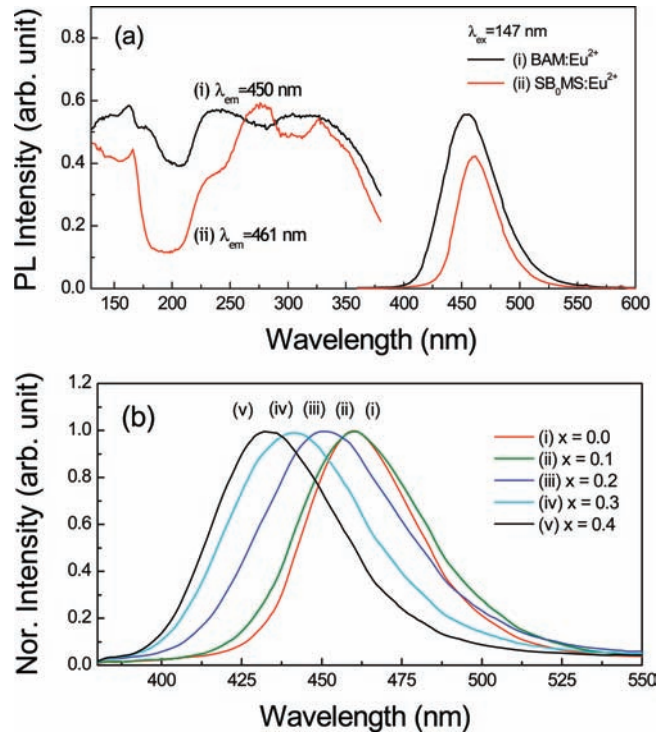

Figure 1. (a) Excitation and emission spectra of $SB_0MS:Eu^{2+}$ phosphor. (b) The emission spectra of $SB_xMS:Eu^{2+}$ with different Ba contents. The insert shows the dependence of peak wavelength on the Ba composition parameter x.

tuned from 434 to 460 nm depending upon the Ba content. For example, at a Ba content of $x = 0.2$, we could obtain a dominant wavelength of 450 nm, similar to that of a commercial $BAM:Eu^{2+}$. As noted earlier with regard to demand for a high degree of performance of PDPs, there is strong demand for high color purity in the development of a blue-emitting phosphor. Therefore, the tunability of the emission wavelength of $SB_xMS:Eu^{2+}$ is a very attractive property for a blue-emitting phosphor.

In order to investigate the aging property under a plasma discharge environment, test panels adopting $BAM:Eu^{2+}$ (commercial) and $SB_{0.2}MS:Eu^{2+}$ phosphors were fabricated by a screen printing process and evaluated in a discharge chamber maintained at 70 torr. The discharge gas was prepared by mixing Xe (10%) and He (90%). The luminescent properties of the panels were measured while driving at 700 V and 20 kHz. The aging characteristics of the phosphors using the test panels are demonstrated in Figure 2. The initial intensities of both phosphor panels decreased due to contamination of the measurement system. However, the aging property of the $SB_{0.2}MS:Eu^{2+}$ phosphor panel was superior to that of the $BAM:Eu^{2+}$ panel. Thus, Xe ion bombardment appears to be rather inconsequential with respect to the deterioration of $SB_{0.2}MS:Eu^{2+}$ in comparison with $BAM:Eu^{2+}$. Thus, $SB_xMS:Eu^{2+}$ could be a good candidate for PDP blue phosphor, since it has a long lifetime under a plasma environment.

In order to investigate their thermal stability after a baking process, the $SB_xMS:Eu^{2+}$ phosphors were baked in the air at 500 °C for 30 min. Figure 3 shows the relative PL intensity of the $SB_xMS:Eu^{2+}$ phosphor samples in accordance with

(17) Larson, A. C.; Von Dreele, R. B. *Report LAUR 86*; Los Alamos National Laboratory: Los Alamos, NM, 1994; p 748.
(18) Payne, M. C.; Peter, M. P.; Allan, D. C.; Arias, T. A.; Joannopoulos, J. D. *Rev. Modern Phys.* **1992**, *64*, 1045.
(19) Perdew, J. P.; Burke, K.; Ernzerhof, M. *Phys. Rev. Lett.* **1996**, *77*, 3865.
(20) Monkhorst, H. J.; Pack, J. D. *Phys. Rev. B: Condens. Matter Mater. Phys.* **1977**, *16*, 1748.
(21) Shinoya, S.; Yen, W. M. *Phosphor Handbook*; CRC Press: Boca Raton, FL, 1998.
(22) Blasse, G. Grabmaier, B. C. *Luminescent Materials*; Springer: New York, 1994.

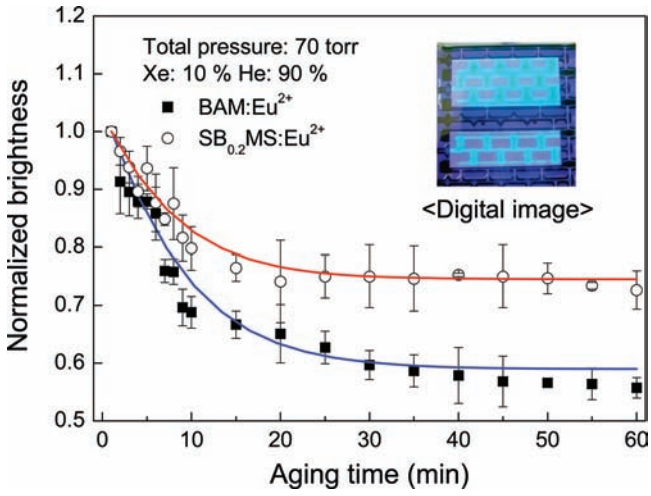

Figure 2. Aging characteristics of test panels of BAM:Eu^{2+} and $SB_{0.2}$MS:Eu^{2+} phosphor.

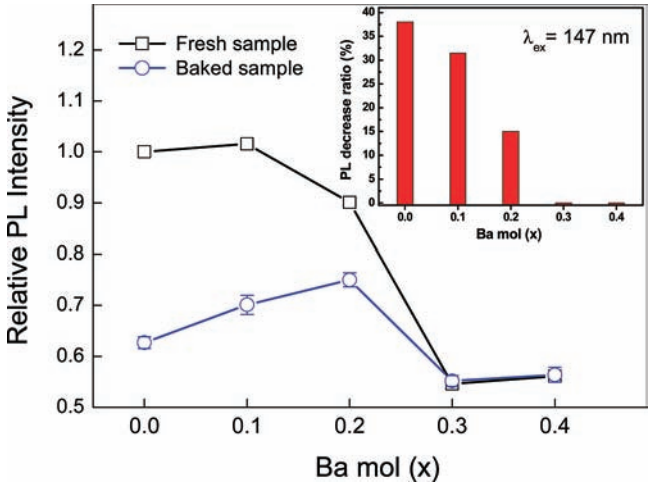

Figure 3. Relative PL intensity of before and after baking process of SB_xMS:Eu^{2+} with various Ba contents.

Ba content after the baking process. In particular, the PL intensity of SB_0MS:Eu^{2+} decreased significantly by as much as 38% of the initial intensity, after the baking process. However, with increasing Ba content, a reduction of the decrease ratio was observed, as shown in Figure 3. When Ba content introduced into the host lattice was above $x = 0.3$, the initial PL intensity of SB_xMS:Eu^{2+} was maintained after the baking process. This means that the addition of Ba to the host lattice significantly affected the thermal stability of the phosphor during the baking process. As noted earlier, the thermal stability of phosphors during the manufacture of PDPs is the most important demand for color-emitting phosphors. Although the PL properties of SB_xMS:Eu^{2+} were excellent in terms of long-term stability under plasma discharge and color purity, SB_xMS:Eu^{2+} was not used as a PDP phosphor. Therefore, it is worth it to investigate the large variation of thermal stability in SB_xMS:Eu^{2+} phosphor samples.

3.2. Analysis of Ba Substitution Sites of SB_xMS:Eu^{2+} Phosphor in Terms of Their Effects on Thermal Stability. 3.2.1. Confirmation of Differences for Eu^{2+} Sites via ESR Analysis. The decrease of the PL intensity of SB_xMS:Eu^{2+} ($x = 0$, 0.1, 0.2) can be attributed to either

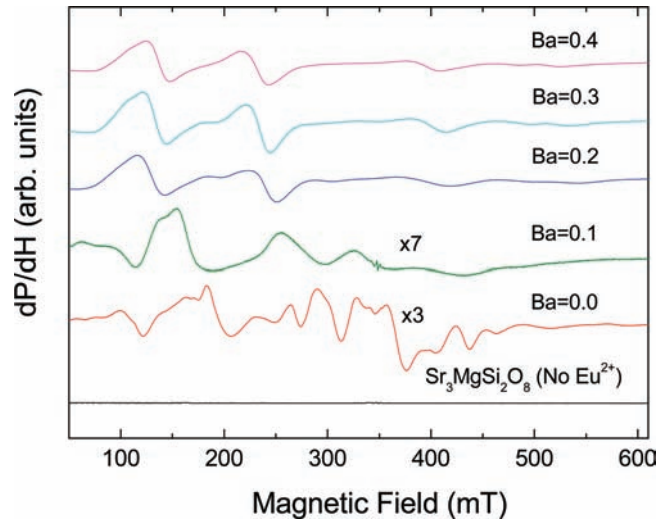

Figure 4. ESR spectra of SB_xMS:Eu^{2+} with various Ba contents.

the lattice degradation or the decrease of Eu^{2+} concentration.[7,13] One of our previous studies showed that lattice degradation of $BaAl_2Si_2O_8$:Eu^{2+} phosphor did not affect its PL intensity in a low-temperature region of about 500 °C.[13] When the neutron powder diffraction (NPD) patterns of fresh SB_xMS:Eu^{2+} were compared with those of SB_xMS:Eu^{2+} baked at 500 °C in the air, no impurity phase was found in either. This result indicates that the concentration change of Eu^{2+} ions which occurs in the air causes a PL intensity decrease of SB_xMS:Eu^{2+}. These Eu^{2+} ions may occupy preferred substitutional sites, which may influence the thermal stability of the phosphor. There are three different Sr sites in the SB_xMS host lattice, and Eu^{2+} ions may occupy substitutable sites depending upon the Ba content.

Bearing this in mind, the behavior of the PL decrease ratio with various Ba contents in SB_xMS:Eu^{2+} after the baking process was investigated via an ESR experiment performed on Eu^{2+} ions of these phosphor samples. The ESR technique can deliver local information about the surroundings of the Eu^{2+} ions, because the ESR signal from Eu^{2+} ions is highly sensitive to different surroundings around Eu^{2+} ions ($4f^7$, $S = 7/2$, $L = 0$, $J = 7/2$).[7,14] Figure 4 depicts the ESR spectra of SB_xMS:Eu^{2+} with various Ba contents. As shown in Figure 4, there are basically three different surroundings of Eu^{2+} in the host lattice: at Ba contents $x = 0$, $x = 0.1$, and from $x = 0.2$ to $x = 0.4$. The difference in the ESR signals can be attributed to either the change of the space group or the change of Eu^{2+} sites in the host lattice with Ba addition. However, when structural refinements were carried out on the SB_xMS:Eu^{2+} phosphor samples, the structural parameters of all samples using the same space group were determined successfully. This indicates that Eu^{2+} ions could occupy the different Sr sites in the host lattice depending upon the Ba content. It is known that there are three different substitutional sites of Eu^{2+} ions in this host lattice. And they have different local structures and crystal fields due to different coordinations and bond lengths between neighboring oxygen and the Sr atoms for each Sr site. Comparing the relative PL decrease ratio with the ESR results, it appears that the

thermal stability of $SB_xMS:Eu^{2+}$ is closely related to the substitutional site of Eu^{2+} in the host lattice.

3.2.2. Selection of Eu^{2+} Substitution Amount for Each Sr Site via Structural Refinement and Quantum Calculation. In order to determine which substitutional site Eu^{2+} ions occupy, NPD analyses were carried out for the $SB_xMS:Eu^{2+}$ phosphor samples. NPD analyses are particularly useful in obtaining information on the oxygen atoms in $SB_xMS:Eu^{2+}$.[24] And NPD can discriminate adjacent atomic species such as Mg^{2+} and Si^{4+} in SB_xMS, because neutron scattering is not dependent upon the number of electrons in an atom. Unfortunately, because the concentration of Eu^{2+} ions in the host lattice was very small in comparison with those of other elements, it was difficult to directly determine which substitutional sites Eu^{2+} ions occupy via any analytical tools. And, Eu content is also independent of Ba content ($= x$) because the solubility limit of Eu^{2+} (>0.18) in the SB_xMS host lattice is a quite large amount compared with the 0.02 of Eu^{2+}. Therefore, to determine the substitutional site of Eu^{2+} for each Sr site, determination of the Ba substitutional site was carried out using the Rietveld refinement method. Because the ionic radius of Ba^{2+} (1.52 Å, $n = 10$) is larger than that of Eu^{2+} (1.35 Å, $n = 10$), Eu^{2+} ions could substitute for Sr^{2+} (1.36 Å, $n = 10$) sites easily.[25] Upon the incorporation of Ba ions into three different sites of Sr^{2+}, Eu^{2+} ions will substitute for Sr^{2+} sites having a similar ionic radius rather than sites occupied by Ba^{2+}, which have a larger ionic radius. Therefore, it is very important to determine Ba substitutional sites in the SB_xMS host lattice depending upon Ba content. In addition, the neutron scattering length between Ba (0.52×10^{-12} cm) and Sr (0.69×10^{-12} cm) is sufficient to discriminate each site occupancy of Ba.

When Ba^{2+} ions are incorporated into the crystal structure of SB_xMS, Ba^{2+} ions may substitute for all cationic sites, that is, Sr^{2+}, Mg^{2+}, and Si^{4+}. However, considering their respective ionic radius and allowed oxygen-coordination number (n), Mg^{2+} (0.72 Å, $n = 6$), Si^{4+} (0.26 Å, $n = 4$), Sr^{2+} (1.36 Å, $n = 10$), and Eu^{2+} (1.35 Å, $n = 10$), it is difficult for Ba^{2+} ions to substitute for Mg^{2+} or Si^{4+} ions.[25] Therefore, the structural refinement proceeded under the assumption that Ba^{2+} ions substituted only for Sr^{2+} sites. The occupancies of the Ba^{2+} and Sr^{2+} sites were constrained such that the total occupancy of Ba^{2+} and Sr^{2+} ions was maintained to be unity depending on the Ba content ($= x$).

Structural refinements were carried out for the $SB_xMS:Eu^{2+}$ phosphor. A reasonable approximation of the actual crystal structure as a starting model is required to perform the crystal structural refinement. The starting structural model for $SB_xMS:Eu^{2+}$ was built with crystallographic data reported by Moore and Araki.[23] Figure 5 shows the crystal structure of SB_0MS and three different Sr sites with their corresponding coordination number. SB_0MS (merwinite), which belongs to a monoclinic space group ($P2_1/a$), consists of a [MgO_6] octahedral and a [SiO_4] tetrahedral group.[23] Sr ions are

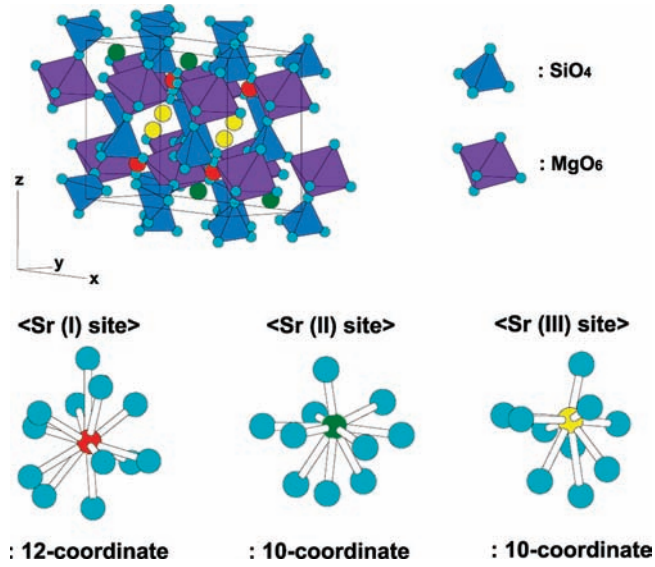

Figure 5. Crystal structure and cation polyhedra arrangements of $SB_xMS:Eu^{2+}$ phosphor.

present at three different sites in a unit cell, that is, 12-coordinated Sr(I), 10-coordinated Sr(II), and Sr(III) sites.

Figure 6 shows Rietveld refinement patterns of $SB_xMS:Eu^{2+}$. The final weighted R factors, R_{wp}, of all samples were successfully converged to a satisfactory level (R_{wp} = 4.39∼5.09%). The refined structural parameters, selected atomic distances, and bond angles of $SB_{0.4}MS:Eu^{2+}$ are listed representatively in Tables 2 and 3. The structural parameters of $SB_xMS:Eu^{2+}$ have been determined successfully by the Rietveld refinement method.

Figure 7a shows the relative amount of substitutional elemental Ba at three different Sr sites as obtained by the Rietveld refinement. As shown in Figure 7a, at a Ba content of $x = 0.1$, the amount of Ba substitution for three Sr sites showed a similar weight between 30 and 35%. This indicates that Ba ions randomly occupied each Sr site in the initial stage. However, with increasing Ba content, the amounts of Ba substitution varied distinctly depending upon the sites, particularly the Sr(I) and Sr(III) sites. Notably, the Sr(III) site had very little substitution by Ba ions at $x = 0.3$ and 0.4. On the basis of the calculated relative amount of substitutional Ba atoms, the occupation probability of Eu^{2+} ions for each given Sr site was defined and estimated as follows:

$$\text{occupation probability of } Eu^{2+}\text{ions for each Sr site} = \frac{\text{Sr mol \% at each site}}{\text{Sr mol \% of (Sr(I) + Sr(II) + Sr(III) site)}}$$

Due to the similar ionic radius between Eu (1.35 Å, $n =$ 10) and Sr (1.36 Å, $n = 10$) atoms, it was initially assumed that Eu^{2+} ions mainly substituted for the Sr site rather than Ba (1.52 Å, $n = 10$). Using the equation defined above, the occupation probabilities of Eu^{2+} ions for each Sr site are listed in Table 4. As shown in Table 4, the occupation probability of Eu^{2+} at the Sr(II) site was not changed with Ba addition. However, in the cases of the Sr(I) and Sr(III) sites, the occupation probability of Eu^{2+} was dramatically changed with increasing Ba content. Therefore, it is evident

(23) Moore, P. B.; Araki, T. *Am. Mineral.* **1972**, *57*, 1355.
(24) Young, R. A. *The Rietveld Method*; Oxford University Press: New York, 1995.
(25) Shannon, R. D. *Acta Crystallogr.* **1976**, *A32*, 751.

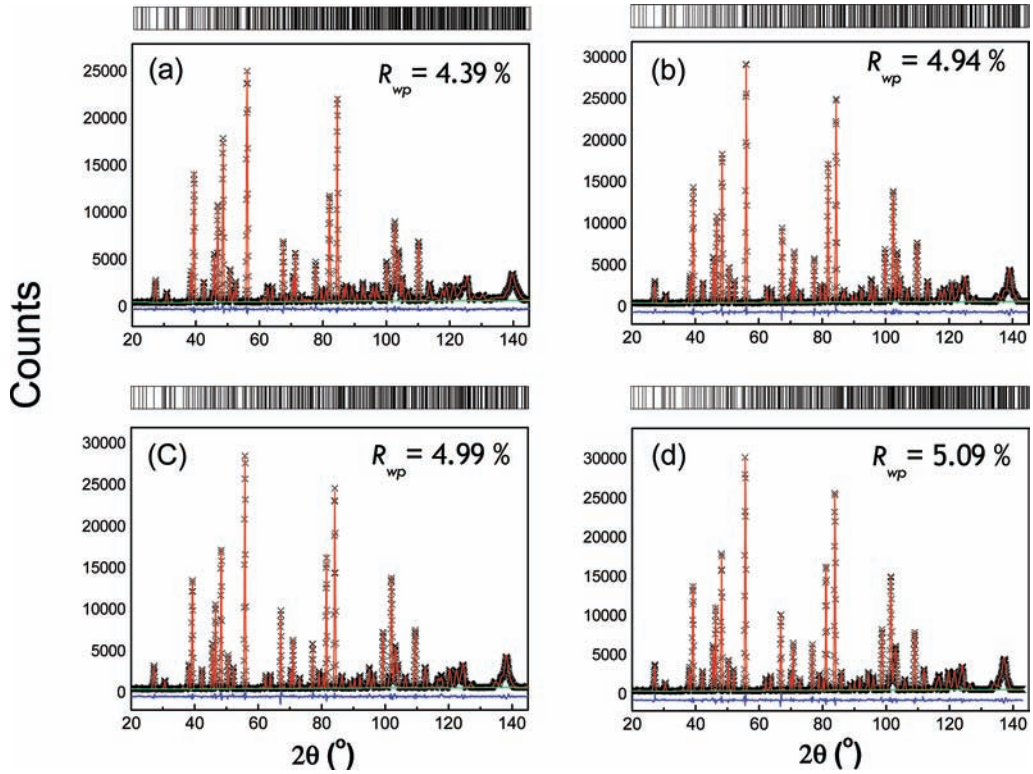

Figure 6. Rietveld refinement patterns for $SB_xS:Eu^{2+}$ NPD data: (a) $x = 0.1$, (b) $x = 0.2$, (c) $x = 0.3$, and (d) $x = 4$. Dot marks represent the observed intensities, and the solid line represents calculated ones. A difference (obsd − calcd) plot is shown beneath. Vertical lines in the top position indicate the reflection positions.

Table 2. Refined Structural Parameters of $SB_{0.4}MS:Eu^{2+}$ Obtained from the Rietveld Refinement Using NPD Data Taken at Room Temperature[a,b,c,d]

		$SB_{0.4}MS:Eu^{2+}$				
atom	position	x	y	z	g^e	$100 \times U_{iso}/Å^{2f}$
Sr (1)	4e	0.2530(8)	0.2501(9)	0.2551(5)	0.203(4)	1.09(5)
Ba (1)	4e	0.2530(8)	0.2501(9)	0.2551(5)	0.797(4)	1.09(5)
Sr (2)	4e	0.0826(9)	0.2457(3)	−0.0880(4)	0.666(4)	0.18(8)
Ba (2)	4e	0.0826(9)	0.2457(3)	−0.0880(4)	0.334(4)	0.18(8)
Sr (3)	4e	0.0804(6)	0.7515(8)	0.4137(3)	0.931(4)	0.40(2)
Ba (3)	4e	0.0804(6)	0.7515(8)	0.4137(3)	0.069(4)	0.40(2)
Mg	4e	−0.0007(1)	0.2434(2)	0.2444(2)	1.0	0.43(6)
Si (1)	4e	0.1359(4)	0.2524(4)	0.5837(7)	1.0	0.12(7)
Si (2)	4e	0.1337(8)	0.7491(2)	0.0807(7)	1.0	0.08(1)
O (1)	4e	0.0896(9)	0.2454(6)	0.4210(4)	1.0	1.41(5)
O (2)	4e	0.0882(2)	0.4865(1)	0.6579(9)	1.0	0.55(6)
O (3)	4e	0.0872(4)	0.0081(4)	0.6586(6)	1.0	0.04(1)
O (4)	4e	0.2466(7)	0.2526(3)	0.5783(7)	1.0	1.15(1)
O (5)	4e	0.0865(8)	0.7531(7)	−0.0756(8)	1.0	1.25(4)
O (6)	4e	0.2504(6)	0.7296(4)	0.0755(2)	1.0	0.65(3)
O (7)	4e	0.0898(6)	0.5072(6)	0.1609(1)	1.0	0.34(3)
O (8)	4e	0.0925(4)	−0.0125(4)	0.1587(5)	1.0	0.30(5)

[a] The numbers in parentheses are the estimated standard deviations of the last significant. [b] Space group: $P2_1/a$ (No.14) $a = 14.0722(1)$ Å, $b = 5.5093(1)$ Å, and $c = 9.9532(1)$ Å. $\alpha = 90°$, $\beta = 90.021°$, and $\gamma = 90°$. [c] Constraint on occupancy: $g(Ba(1)) + g(Sr(1)) = g(Ba(2)) + g(Sr(2)) = g(Ba(3)) + g(Sr(3)) = 1$, $g(Ba(1)) + g(Ba(2)) + g(Ba(3)) = 1.2$. [d] Constraint on isotropic atomic displacement factor: $U_{iso}(Ba(1)) = U_{iso}(Sr(1))$, $U_{iso}(Ba(2)) = U_{iso}(Sr(2))$, $U_{iso}(Ba(3)) = U_{iso}(Sr(3))$. [e] Occupation factor. [f] Isotropic atomic displacement factor.

that the amount of Eu^{2+} ions in the Sr(I) and Sr(III) sites plays an important role in the thermal stability. The proposed mechanism that Eu^{2+} ions occupy substitutional sites selectively depending on Ba content is schematically illustrated in Figure 8. As noted in earlier results pertaining to ESR with various Ba contents, there are basically three different surroundings of Eu^{2+} in the host lattice. The effect of the amount of Ba substitution for Sr sites showed good agreement with the ESR results. Consequently, the difference in the thermal stability of $SB_xMS:Eu^{2+}$ with various Ba contents could be explained by the preference of Eu^{2+} for Sr sites. The difference in Eu^{2+} substitution site serves as a shield for Eu^{2+} against the oxidizing atmosphere during the baking process.

Through our previous study utilizing a polymorph of $BaAl_2Si_2O_8:Eu^{2+}$, it was suggested that two criteria could be used in selecting a host lattice showing thermal stability during the baking process, d_{Eu-O} and a non-open-structure.[13] The average interatomic length was thus calculated to quantitatively confirm the sensitivity of Eu^{2+} ions to the outer oxidizing atmosphere on the basis of a Rietveld refinement. From the Rietveld refinement results shown in Figure 7b and

Table 3. Selected Interatomic Distances and Bond Angles for $SB_{0.4}MS:Eu^{2+}$ at Room Temperature

$SB_{0.4}MS:Eu^{2+}$							
distance (Å)		angle (deg)		distance (Å)		angle (deg)	
Tetrahedron Coordination							
Si(1)−O(1)	1.682(1)	O(1)−Si(1)−O(2)	105.1(1)	Si(2)−O(5)	1.632(2)	O(5)−Si(2)−O(6)	112.2(1)
Si(1)−O(2)	1.617(1)	O(1)− Si(1)−O(3)	102.5(1)	Si(2)−O(6)	1.646(1)	O(5)− Si(2)−O(7)	106.2(2)
Si(1)−O(3)	1.670(2)	O(1)−Si(1)−O(4)	110.8(1)	Si(2)−O(7)	1.655(2)	O(5)−Si(2)−O(8)	105.2(1)
Si(1)−O(4)	1.559(2)	O(2)− Si(1)−O(3)	106.5(1)	Si(2)−O(8)	1.616(2)	O(6)−Si(2)−O(7)	109.5(1)
		O(2)−Si(1)−O(4)	115.4(1)			O(6)−Si(2)−O(8)	115.1(2)
		O(3)−Si(1)−O(4)	115.1(1)			O(7)−Si(2)−O(8)	107.9(1)
Octahedron Coordination							
Mg(1)−O(1)	2.109(2)	O(1)−Mg(1)−O(2)	89.7(2)			O(2)−Mg(1)−O(7)	91.8(2)
Mg(1)−O(2)	2.103(2)	O(1)−Mg(1)−O(2)	90.1(1)			O(2)−Mg(1)−O(8)	175.9(1)
Mg(1)−O(3)	2.063(1)	O(1)−Mg(1)−O(2)	179.1(1)			O(3)−Mg(1)−O(5)	90.5(2)
Mg(1)−O(5)	2.011(1)	O(1)−Mg(1)−O(2)	86.1(1)			O(3)−Mg(1)−O(7)	175.7(2)
Mg(1)−O(7)	2.091(1)	O(1)−Mg(1)−O(2)	86.3(2)			O(3)−Mg(1)−O(8)	95.2(2)
Mg(1)−O(8)	2.092(2)	O(2)−Mg(1)−O(3)	86.1(1)			O(5)−Mg(1)−O(7)	93.1(2)
		O(2)−Mg(1)−O(5)	89.7(1)			O(5)−Mg(1)−O(8)	94.0(2)
						O(7)−Mg(1)−O(8)	86.4(1)
12-Coordinated Polyhedron: Sr(I) Site		10-Coordinated Polyhedron: Sr(II) Site		10-Coordinated Polyhedron: Sr(III) Site			
Sr(1)−O(1)	2.791(1)	Sr(2)−O(2)	2.761(2)	Sr(3)−O(1)	2.792(1)		
Sr(1)−O(2)	2.789(2)	Sr(2)−O(3)	2.747(1)	Sr(3)−O(1)	2.724(2)		
Sr(1)−O(3)	2.782(1)	Sr(2)−O(5)	2.716(2)	Sr(3)−O(1)	2.866(1)		
Sr(1)−O(4)	3.082(1)	Sr(2)−O(5)	2.798(2)	Sr(3)−O(2)	2.750(1)		
Sr(1)−O(4)	3.167(1)	Sr(2)−O(5)	2.848(1)	Sr(3)−O(2)	2.796(2)		
Sr(1)−O(4)	3.190(2)	Sr(2)−O(6)	2.352(2)	Sr(3)−O(3)	2.730(2)		
Sr(1)−O(5)	2.831(1)	Sr(2)−O(7)	2.778(1)	Sr(3)−O(3)	2.792(1)		
Sr(1)−O(6)	3.340(1)	Sr(2)−O(7)	2.868(2)	Sr(3)−O(4)	2.433(2)		
Sr(1)−O(6)	3.148(1)	Sr(2)−O(8)	2.752(2)	Sr(3)−O(7)	2.763(2)		
Sr(1)−O(6)	3.154(1)	Sr(2)−O(8)	2.860(2)	Sr(3)−O(8)	2.761(1)		
Sr(1)−O(7)	2.843(2)						
Sr(1)−O(8)	2.835(2)						

Table 3, the average interatomic length between Eu^{2+} and the oxygen (d_{Eu-O}) of the Sr sites dramatically changed depending on the Ba content (= x) due to the site preference of Ba. In particular, the d_{Eu-O} in $SB_{0.4}MS:Eu^{2+}$ was 2.741(2) Å in the Sr(III) site, while the d_{Eu-O} values of the Sr(I) and Sr(II) sites are 2.996(1) Å and 2.748(2) Å, respectively. The difference in d_{Eu-O} values of the Sr sites supports Eu^{2+} ions substituting the Sr(I) and(II) sites possibly being more sensitive to the external environmental conditions.

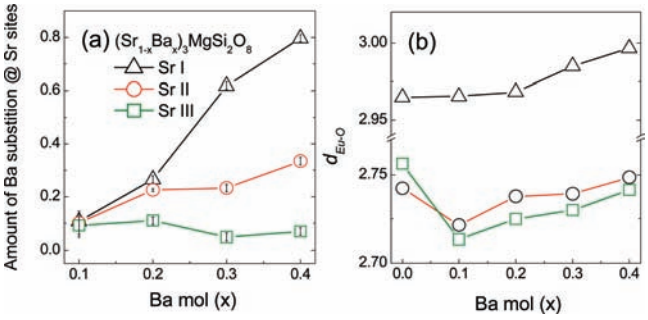

Figure 7. (a) Relative amount of Ba substitution at three different Sr sites against NPD and (b) interatomic distances between Eu^{2+} and O^{2-} (d_{Eu-O}) depending on Ba content (= x).

Table 4. Calculated Occupation Probability of Eu^{2+} Ions for Occupying Each Sr Site of $SB_xMS:Eu^{2+a}$

	occupation probability of Eu^{2+} (%)		
Ba mol (x)	Sr(I) site	Sr(II) site	Sr(III) site
0.1	33	33	34
0.2	31	32	37
0.3	18	37	45
0.4	11	37	52

[a] Occupation probability of Eu^{2+} (%).

To confirm the results showing preferred Ba substitution sites obtained by the Rietveld refinement using NPD, we carried out a quantum calculation based on the CASTEP program. For the calculation of total energy, we assumed the following two conditions: (1) Ba ions are substituted for one or two Sr sites completely, and (2) as the total energy of the system is lowered, the site in the host lattice becomes accordingly more stable. Table 5 shows the calculated total energy of each given Sr site substituted with Ba atoms. Among the three Sr sites substituted with Ba, the Sr(I) site was the most stable. Furthermore, Sr(I) and Sr(II) sites had the lowest total energy for the given combination of Sr sites. The Rietveld refinement result agreed very well with the total

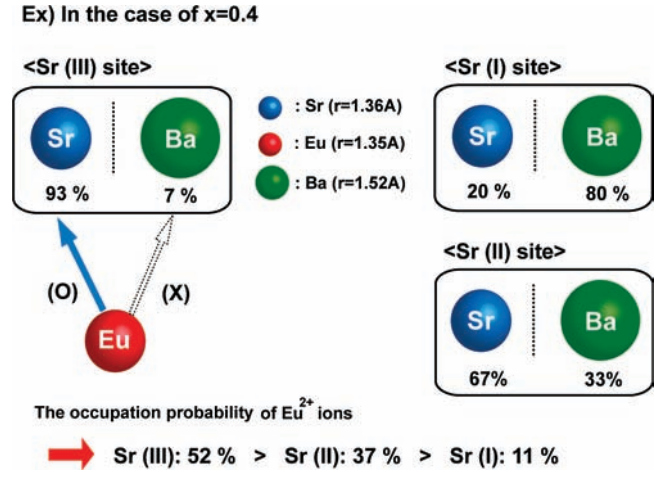

Figure 8. Schematic diagram of proposed model for thermal stability depending upon Ba content.

Table 5. Calculated Total Energy of SB_xMS System for Occupying Each Substitutional Site with the Ba Atom

replaced atomic site	replacing atom	energy (eV)
Sr(III)	Ba	-2.84324988×10^4
Sr(II)	Ba	-2.84348694×10^4
Sr(I)	Ba	-2.84348743×10^4
Sr(I), Sr(II)	Ba,Ba	-2.78859816×10^4
Sr(II), Sr(III)	Ba,Ba	-2.78833882×10^4
Sr(I), Sr(III)	Ba,Ba	-2.78859623×10^4

Table 6. Selected Bond Angles of O−Sr−O for $SB_{0.4}MS:Eu^{2+}$ at Room Temperature

Sr(II) site	angle (deg)	Sr(III) site	angle (deg)
O(2)−Sr(2)−O(3)	57.165(1)	O(1)−Sr(3)−O(2)	56.416(1)
O(2)−Sr(2)−O(5)	63.674(1)	O(1)−Sr(3)−O(3)	119.599(1)
O(2)−Sr(2)−O(6)	91.957(4)	O(1)−Sr(3)−O(4)	87.427(0)
O(2)−Sr(2)−O(7)	65.420(3)	O(1)−Sr(3)−O(7)	62.170(1)
O(2)−Sr(2)−O(8)	91.933(3)	O(1)−Sr(3)−O(8)	119.276(1)
O(3)−Sr(2)−O(5)	64.006(1)	O(2)−Sr(3)−O(3)	63.242(2)
O(3)−Sr(2)−O(6)	90.176(4)	O(2)−Sr(3)−O(4)	86.315(3)
O(3)−Sr(2)−O(7)	91.905(3)	O(2)−Sr(3)−O(7)	118.534(2)
O(3)−Sr(2)−O(8)	66.380(3)	O(2)−Sr(3)−O(8)	172.970(0)
O(5)−Sr(2)−O(6)	86.564(0)	O(3)−Sr(3)−O(4)	86.429(3)
O(5)−Sr(2)−O(7)	56.304(1)	O(3)−Sr(3)−O(7)	174.845(0)
O(5)−Sr(2)−O(8)	56.332(1)	O(3)−Sr(3)−O(8)	120.449(1)
O(6)−Sr(2)−O(7)	86.574(3)	O(4)−Sr(3)−O(7)	88.850(4)
O(6)−Sr(2)−O(8)	83.525(3)	O(4)−Sr(3)−O(8)	87.950(4)
O(7)−Sr(2)−O(8)	55.004(1)	O(7)−Sr(3)−O(8)	57.225(1)

energy of the system on the basis of the quantum calculation. We also considered variation of the total energy for the given system with Sr sites substituted with Ba atoms. As shown in Figure 5 and Table 3, the Sr(I) site is located in a relatively open place (longer d_{Eu-O}) among the three Sr sites of SB_xMS. As a result, the Sr(I) site is the most stable site in SB_xMS with increasing Ba content. However, both the Sr(II) and Sr(III) sites showed a similar value of d_{Eu-O}. Although there is only a slight difference between the Sr(II) and Sr(III) sites in terms of d_{Eu-O}, their atomic coordination and the angle between Eu^{2+} and neighboring oxygen showed large differences, as shown in Table 6. The difference in O−Sr−O angles supports the data indicating that the Sr(II) environment appears more isotropic than the Sr(III) one; it may explain Ba preference for the Sr(II) site. Therefore, it was demonstrated that preferential occupation of a given Sr site among three possible Sr sites occurs in SB_xMS with Ba addition.

Conclusion

The thermal stability of a blue-emitting $SB_xMS:Eu^{2+}$ phosphor, synthesized by a conventional solid-state reaction, has been evaluated. The improvement in the thermal stability with Ba addition can be ascribed to both the preference of Ba to occupy Sr sites and the average interatomic length between the Eu^{2+} ion and the neighboring oxygen ions (d_{Eu-O}). Through various experimental results, we could infer that the Ba substitution on preferential Sr sites leads to the repulsion of Eu^{2+} ions on low-coordinated and smaller Sr sites and favors the thermal stability of the phosphor. Thus, due to the increase of occupation probability of Eu^{2+} for a Sr site having a shorter d_{Eu-O}, the thermal stability of the phosphor changed dramatically depending upon the amount of Ba content. Consequently, thermal stability can be enhanced via the change of a Eu^{2+} site having a short d_{Eu-O} through the substitution of an element of the host lattice.

Acknowledgment. This study was partially supported by the Korea Science and Engineering Foundation (KOSEF) and the Ministry of Science & Technology (MOST) of the Korean government through its National Nuclear Technology Program and KOSEF grant funded by the Korea government (MOST) (No.2007-00467). The authors are grateful to Dr. Y. N. Choi at the Hanaro Center in Korea Atomic Energy Research Institute for his assistance in collecting neutron powder diffraction data, and also Mr. J. H. Ryu at KAIST for his fruitful discussion on the DFT calculation.

IC8012798